Structure and Magnetism in $Sr_{1-x}A_xTcO_3$ Perovskites. The importance of the A-site cation.

Emily Reynolds

Inorganic Chemistry Laboratory, University of Oxford, South Parks Road, OX1 3QR UK

Maxim Avdeev and Gordon J. Thorogood

Australian Nuclear Science and Technology Organisation, Lucas Heights, NSW 2234 Australia,

Frederic Poineau and Kenneth R Czerwinski

University of Nevada Las Vegas, Department of Chemistry and Biochemistry, 4505 Maryland Parkway, 89154 Las Vegas, NV USA

Justin A. Kimpton

Australian Synchrotron, 800 Blackburn Rd, Clayton, Victoria 3168, Australia.

Michelle Yu, Paula Kayser and Brendan J. Kennedy

School of Chemistry, The University of Sydney, Sydney, NSW 2006 Australia

Abstract

The $Sr_{1-x}Ba_xTcO_3$ (x = 0, 0.1, 0.2) oxides were prepared and their solid-state and magnetic structure studied as a function of the temperature by x-ray and neutron powder diffraction. The refined Tc moments at room temperature and Nèel temperatures for $Ba_{0.1}Sr_{0.9}TcO_3$ and $Ba_{0.2}Sr_{0.8}TcO_3$ were 2.32(14) μ_β and 2.11(13) μ_β and 714 °C and 702 °C respectively. In contrast to expectations, the Nèel temperature in the series $Sr_{1-x}A_xTcO_3$ decreases with increasing Ba content. This observation is consistent with previous experimental measurements for the two series AMO_3 (M = Ru, Mn; A = Ca, Sr, Ba) where the maximum magnetic ordering temperature was observed for A = Sr. Taken with these previous results the current work demonstrates the critical role of the A-site cation in the broadening of the π^* bandwidth and ultimately the magnetic ordering temperature.

Introduction

Strontium technetate, $SrTcO_3$, has emerged as an important case-study in understanding the condensed matter science of 4*d* and 5*d* metal oxides [1-4]. At room temperature it, like its lighter Mn analogue $SrMnO_3$, exhibits a G-type antiferromagnetic arrangement [4, 5]. Both structures are built on corner sharing MO_6 octahedra, although cooperative tilting of the octahedra lowers the symmetry in $SrTcO_3$ [6] to the orthorhombic $GdFeO_3$-type structure. While $SrMnO_3$ (Mn^{4+} $3d^4$) has an unexceptional Nèel temperature (T_N ~ 233 K), the Nèel temperature in $SrTcO_3$ (Tc^{4+} $4d^3$) is exceptionally high T_N ~ 1000 K [4]. Remarkably, the magnetic moment of the Tc (~ 2.1 μ_β at 3K) is smaller than that seen at the same temperature in $SrMnO_3$ ~ 2.6 μ_β [5]. Strontium ruthenate, $SrRuO_3$ (Ru^{4+} $4d^4$), is isostructural with $SrTcO_3$ but is ferromagnetic with a Curie temperature (T_C) of ~ 160 K[7, 8]. The $5d^3$ oxide $NaOsO_3$ is a Curie-Weiss metal at high temperature and transforms to an antiferromagnetically insulating state on cooling to 410 K[9]. The large observed variation in electronic properties is a consequence of the nature of the 4*d* and 5*d* orbitals, which are more extended than that of the 3*d*, resulting in a delicate balance between localised and correlated *d*-electrons.

Prior to the discovery of antiferromagnetism (AFM) persisting to very high temperatures in $SrTcO_3$ (T_N ~ 1000 K) [4] and $CaTcO_3$ (T_N ~ 800 K)[10] , it was generally accepted that the more extended 4*d* and 5*d* orbitals tended not to support strong magnetic exchange, relative to the 3*d* oxides. It is now understood that strong hybridisation between metal 4*d* and O 2*p* states, when the t_{2g} orbitals are half filled $(t_{2g})^3(e_g)^0$, results in strong covalence of the Tc-O interaction which in turn results in exceptionally strong magnetic exchange parameters[11].

A challenge in the study of the fascinating magnetic properties of $SrTcO_3$ is that all known isotopes of Tc are radioactive; this limits the number of experimentally well studied Tc oxides that can be used to benchmark the numerous theoretical studies[3, 12-16]. The unique physical properties of $SrTcO_3$ however justify overcoming the challenges of working with radioactive material. One approach to further our understanding of the origin of the high Nèel temperature in $SrTcO_3$ is to experimentally study the effect of *A*-site doping on the magnetic properties. Structurally, $CaTcO_3$ is more distorted than $SrTcO_3$, reflecting the smaller size of the Ca^{2+} cation relative to Sr^{2+}. Distortion of the TcO_6 octahedra, together with a decrease in the Tc-O-Tc bond angle, is expected to reduce the 4*d* bandwidth and

suppress the kinetic energy gain relative to the formation of the magnetic states. This can explain the higher Nèel temperature in $SrTcO_3$ compared to $CaTcO_3$.

Calculations have predicted [11, 17] that $BaTcO_3$ would have a yet higher Nèel temperature, as the larger Ba^{2+} cation will favour an even less distorted structure and larger Tc-O-Tc bond angle, and hence a stronger superexchange interaction. Considering that the perovskite tolerance factor *t* of $BaTcO_3$ is greater than 1, it is possible that the stable structure of $BaTcO_3$ may be cubic or hexagonal; a similar phenomenon has been observed for $SrMnO_3$ ($t = 1.04$)[18]. Indeed the very limited literature indicates that, when formed at ambient pressure, $BaTcO_3$ adopts an edge sharing hexagonal [19]. Nevertheless, exploring the structure and magnetic properties of the series $Sr_{1-x}A_xTcO_3$ (*A* = Ca, Ba) provides a means to establishing if tuning the $SrTcO_3$ structure by *A*-site doping allows the Nèel temperature to be increased over that seen for $SrTcO_3$. In the present work, we establish how much Ba can be incorporated into the orthorhombic $SrTcO_3$ structure. The resulting samples have been characterised using Synchrotron X-Ray Diffraction (S-XRD), Tc K-edge X-ray absorption spectroscopy and, in selected cases, their magnetic ordering temperature established using neutron powder diffraction (NPD).

Results

(i) Experimental

Caution! ^{99}Tc is a β- emitter (E_{max} = 0.29 MeV). All manipulations were performed in a laboratory designed for radioactivity using efficient HEPA-filtered fume hoods, and following locally approved radiochemistry handling and monitoring procedures. Laboratory coats, disposable gloves, and protective eyewear were worn at all times.

The $Sr_{1-x}Ba_xTcO_3$ (x = 0, 0.1, 0.2, 0.3, 0.4) oxides were prepared at UNLV by mixing and grinding stoichiometric amounts of $SrCO_3$, $BaCO_3$ and TcO_2. The resulting mixtures were placed in a quartz boat and treated at 900 °C for 45 hrs under flowing argon. Intermittent re-grindings were performed in order to optimize the formation of single phase sample. The resulting black powders were initially characterised using laboratory Powder X-ray Diffraction (PXRD). Such measurements established that the maximum Ba-content the structure could accommodate under these conditions was 40%. Attempts at the synthesis of $Ba_{0.5}Sr_{0.5}TcO_3$ were unsuccessful, and resulted in the formation of separate Ba and Sr technetate phases (see Supporting Information (SI). It is possible that alternate synthetic methods, such as high pressure or sol-gel, may extend the range extent of Ba doping in the

series to above x = 0.4, and may reduce the extent of phase separation, however it was not possible to explore these within our laboratories due to the radioactive nature of Tc.

The preparation of larger samples (~1.2-2 g) for neutron measurements was only achieved for x = 0.1 and 0.2 samples and for $Sr_{0.5}Ca_{0.5}TcO_3$. Attempted synthesis of larger samples with higher Ba compositions were unsuccessful with the conventional PXRD measurements showing evidence for bulk phase separation (see SI). Consequently, the x = 0.1 and x = 0.2 Ba doped samples are the focus of this study. A single phase sample of $Sr_{0.5}Ca_{0.5}TcO_3$ (~ 2g) was prepared at ANSTO using the procedure described previously for $SrTcO_3$ [10]; this method did not yield single phase $BaTcO_3$.

Synchrotron X-ray powder diffraction (S-XRD) data were collected over the angular range $5 < 2\theta < 85°$, using X-rays of wavelength 0.82465 Å, on the powder diffractometer at BL-10 beamline of the Australian Synchrotron [20]. The samples were housed in 0.2 mm diameter capillaries that were rotated during the measurements. For neutron diffraction measurements the samples were sealed in 5 mm diameter vanadium cans and neutron powder diffraction (NPD) data were obtained using the high resolution powder diffractometer Echidna at ANSTO's OPAL facility at Lucas Heights [21]. The wavelengths of the incident neutrons, obtained using (335) and (331) reflections of a germanium monochromator, were 1.6220 Å and 2.4395 Å, respectively, as determined using data collected for a certified NIST SRM660b LaB_6 standard. This instrument has a maximum resolution of $\Delta d/d \sim 1 \times 10^{-3}$. X-ray absorption near edge structure (XANES) spectra were collected at the Tc K-edge on beamline 12 at the Australian Synchrotron in transmission mode using argon-filled ionisation chambers[22].

(ii) Crystal Structures

Synchrotron XRD data were collected for the various $Sr_{1-x}A_xTcO_3$ oxides at room temperature. Examination of the S-XRD profiles of the Ba doped samples suggested these to be orthorhombic, however there was no evidence for any *M*-point reflections that are diagnostic of in-phase tilting of the corner sharing TcO_6 octahedra [23]. Under identical conditions we observed M-point reflections in the S-XRD profiles of undoped $SrTcO_3$. Likewise there was no evidence for *M*-point reflections in the NPD pattern of the $Sr_{1-x}Ba_xTcO_3$ (x = 0.1, 0.2) samples, demonstrating the structures cannot be in *Pnma*. Attempts to fit the data for the four Ba containing samples in the alternate orthorhombic space group *Imma*, which forms in $SrTcO_3$ upon heating [6], were unsuccessful. Scrutiny of the diffraction

data indicated that samples were actually a mixture of two phases. A model containing both an orthorhombic *Imma* and tetragonal *I*4/*mcm* phase was developed and this provided a satisfactory fit to the S-XRD data measured at room temperature, see Figure 1.

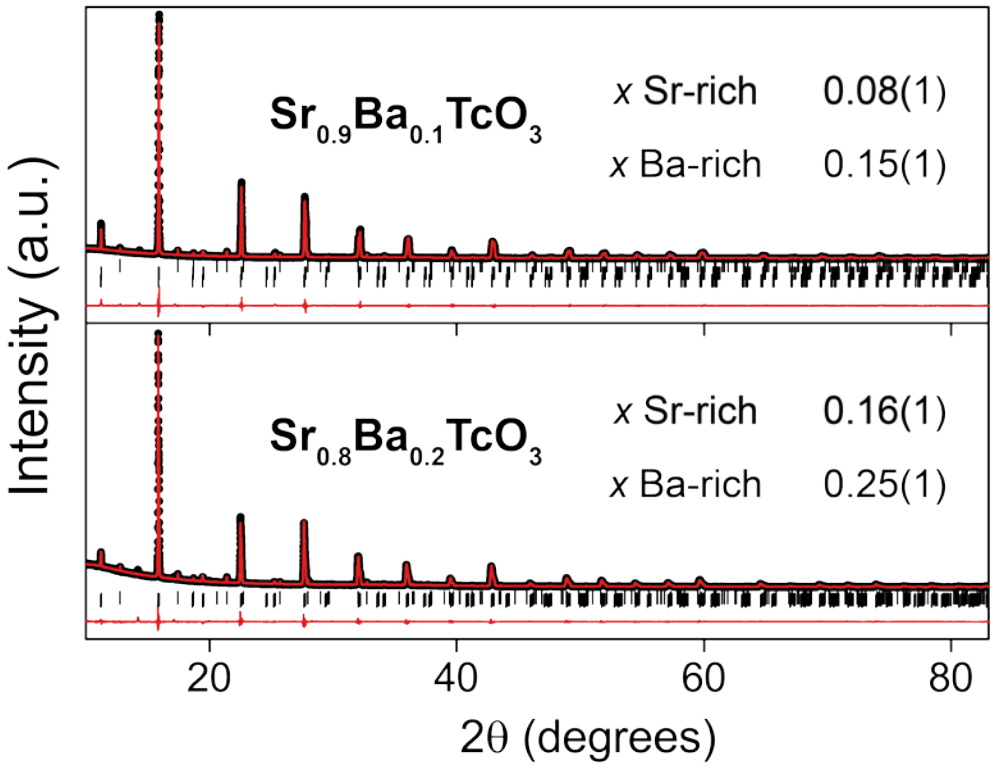

Figure 1. Synchrotron diffraction profiles for $Sr_{0.9}Ba_{0.1}TcO_3$ and $Sr_{0.8}Ba_{0.2}TcO_3$ collected at room temperature. The symbols are the observed data and the solid line the calculated data. The difference between these is shown as a continuous line. There is an impurity Al_2O_3 phase from the mortar used for mixing the reactants. The refined compositions of the two phases (one Sr-rich and one Ba-rich, relative to the ideal composition) are shown above each data set.

Phase separation, involving co-existence of orthorhombic *Imma* and tetragonal *I*4/*mcm* structures, has been observed in a number of perovskites including $SrTcO_3$ [6] and $SrRuO_3$ [24] upon heating and at room temperature in a number of solid solutions including complex manganites of the type $Sr_{1-x}Pr_xMnO_3$ [25] and in $BaPb_{1-x}Bi_xO_3$ at the superconducting composition [26]. It was established that each $Sr_{1-x}Ba_xTcO_3$ sample contains two phases of slightly different compositions, one with a higher than ideal Ba content and the other with a greater than ideal Sr content. Although the Ba content is less than 50% the former is Ba-rich

compared to the ideal composition. In each case the Ba-rich sample will have the larger tolerance factor and this leads to the stabilisation of the tetragonal structure. The results of this analysis are summarised in Table 1. The composition of two phases within each sample was established by refining the site occupancies against the S-XRD data over a range of temperatures, including room temperature and in the high temperature cubic region (see below). For each sample the phase containing more Sr was observed to have a smaller cell volume, reflecting the difference in the size of the two cations, and lower symmetry. The latter reflects the smaller tolerance factors which are correlated with the introduction of cooperative tilting in perovskites. That the tetragonal structure exists in the $x = 0.1$ sample with a refined Ba content of 0.16(1) and a sample with effectively the same amount of Ba (0.15(1) in the x = 0.2 sample has an orthorhombic structure represents both the limitations of Rietveld refinements to accurately and precisely establish this and the sensitivity of the transition. Table 2 gives the refined structural parameters for one example ($x = 0.2$). The S-XRD profiles of the various Ba doped samples were noticeably broader than that observed for $SrTcO_3$, suggesting the domains of the phase separated compositions are relatively small. Further details are given in the supplementary material. XAS measurements at the Tc K-edge demonstrated the Tc to be tetravalent in all cases, Figure 2.

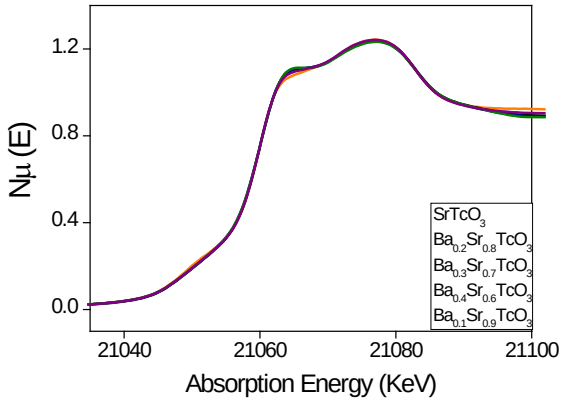

Figure 2. Normalized K K-edge XANES spectra collected from various Ba doped $Sr_{1-x}Ba_xTcO_3$ samples at room temperature.

Ideal *x*	***x* in Sr-rich phase**	**%**	**Space Group**	**Vol. (Å^3)**	***x* in Ba-Rich Phase**	**%**	**Space Group**	**Vol. (Å^3)**
0.1	0.08(1)	80(1)	*Imma*	247.68	0.16(1)	20(1)	*I*4/*mcm*	*250.28*
0.2	0.15(1)	47(1)	*Imma*	247.76	0.25(1)	53(1)	*I*4/*mcm*	*250.43*
0.3	0.17(1)	73(1)	*Imma*	248.70	0.35(1)	27(1)	*I*4/*mcm*	*250.63*
0.4	0.19(1)	42(1)	*Imma*	249.78	0.45(1)	58(1)	*Pm*3*m*	*251.30*

Table 1. Cation occupancy and phase abundance in the $Ba_xSr_{1-x}TcO_3$ samples established by Rietveld refinements against S-XRD data. In all cases the lower symmetry orthorhombic phase has a small volume and lower Ba content.

Composition	**$Ba_{0.15}Sr_{0.85}TcO_3$**	**$Ba_{0.25}Sr_{0.75}TcO_3$**
Space Group	*Imma*	*I*4/*mcm*
Weight %	47.0(1)	53.0(1)
a (Å)	5.58517(8)	5.6146(7)
b (Å)	7.9067(2)	= *a*
c (Å)	5.605(2)	7.9443(3)
Ba/Sr	4*e* (0 ¼ *z*)	4*b* (0 ½ ¼)
z	0.498(2)	
B_{iso} (Å^2)	1.11(3)	1.03(2)
Tc	4*a* (0 0 0)	4*c* (0 0 0)
B_{iso} (Å^2)	0.39(2)	0.20(1)
O1	4*e* (0 ¼ *z*)	4*a* (0 0 ¼)
z	0.046(4)	
B_{iso} (Å^2)	0.5(4)	0.8(7)
O2	8*g* (¼ *y* ¼)	8*h* (*x x* + ½ 0)
x/y	0.511(3)	0.244(5)
B_{iso} (Å^2)	1.1(2)	0.7(4)

Table 2: Refined structural parameters for $Ba_{0.2}Sr_{0.8}TcO_3$ from SXRD data recorded at room temperature, with $R_p = 0.033$ and $R_{wp} = 0.046$.

The temperature dependence of the structures was determined using SXRD. The appropriate space group was established through examination of the diagnostic splitting of the primitive perovskite reflections such as the $(222)_p$ and the nature of any superlattice reflections. For example the evolution of the 112/211/031 multiplet showed that an *Imma* → *I*4/*mcm* transition occurred near 300 °C in the $x = 0.1$ sample. The 211 and 031 reflections overlap such that what is a single reflection (121) in the tetragonal structure appears as a doublet in the *Imma* orthorhombic structure. Once the appropriate space groups were established the structures were refined by the Rietveld method. The temperature dependence of the lattice parameters are shown in Figure 3. Each sample undergoes the same sequence of phase transitions as observed for the $SrTcO_3$ end-member [6], save none exhibited the *Pnma* structure observed for undoped $SrTcO_3$ at room temperature, $Imma(a^-a^-c^0) \rightarrow I4/mcm(a^0a^0c^-) \rightarrow Pm3m(a^0a^0a^0)$, where the corresponding Glazer tilt system is given in parenthesis. This sequence of structures is a consequence of the systematic loss of the in-phase tilts of the corner sharing TcO_6 octahedra upon heating and is frequently observed in perovskites [27]. The co-existence of the two phases was most easily observed by examination of the high temperature S-XRD profiles where both phases adopted a cubic structure (see SI).

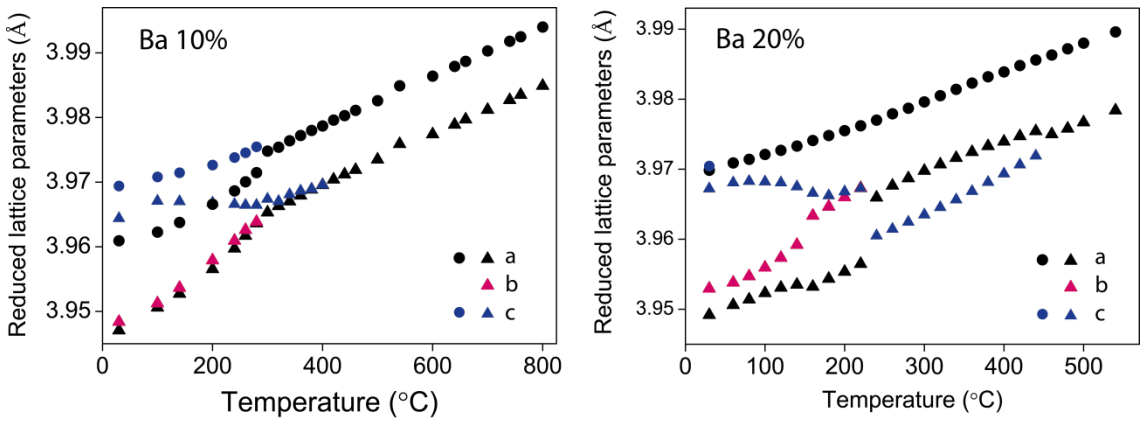

Figure 3. Temperature dependence of lattice parameters of $Ba_xSr_{1-x}TcO_3$ ($x = 0.1, 0.2$) estimated from Rietveld analysis of synchrotron XRD data. The triangle and circle markers correspond to the Sr- and Ba-rich phase (relative to the ideal composition) for each sample.

(iii) Magnetic Structures

Since it was not possible to prepare samples of $Ba_{0.3}Sr_{0.7}TcO_3$ and $Ba_{0.4}Sr_{0.6}TcO_3$ in sufficient quantities for NPD measurements, NPD data was collected only for the samples with the lowest Ba content, $Ba_{0.1}Sr_{0.9}TcO_3$ and $Ba_{0.2}Sr_{0.8}TcO_3$. In addition the mixed Ca-Sr oxide $Ca_{0.5}Sr_{.5}TcO_3$ was also studied by PND between room temperature and 900 °C. These data are compared here with the results obtained previously for $SrTcO_3$ [4]. Examination of the room temperature NPD patterns of these four samples revealed appreciable intensity in the orthorhombic (110) reflection near $2\theta = 20°$ (d = 4.57Å) as a consequence of magnetic ordering (examples of the refinements shown in Figures 4 and 5). That only one strong magnetic peak is observed, reflects the rapid decrease in intensity with increasing 2θ for 4*d* and 5*d* electrons, due to their delocalised nature [28]. The magnetic contribution to the NPD data was fitted using a G-type AFM magnetic structure, as established previously for $SrTcO_3$ and $CaTcO_3$ [4, 10]. In this arrangement, the spin on each cation is aligned anti-parallel to those on all six of its nearest neighbours. Phase separation was not apparent in the NPD patterns of the two Ba containing oxides, presumably due to the lower peak-shape resolution of the NPD. Consequently the structures were refined against combined S-XRD and NPD data sets. The model included two nuclear phases, corresponding to the Ba-rich and Sr-rich compositions described above, and a corresponding magnetic cell. Since the magnetic structure was found to be independent of crystal structure in $SrTcO_3$ [6], the same magnetic structure was used for both compositions. Phase separation was not observed in the S-XRD profile for $Ca_{0.5}Sr_{0.5}TcO_3$ and consequently the crystal and molecular structure of this was refined using NPD data alone.

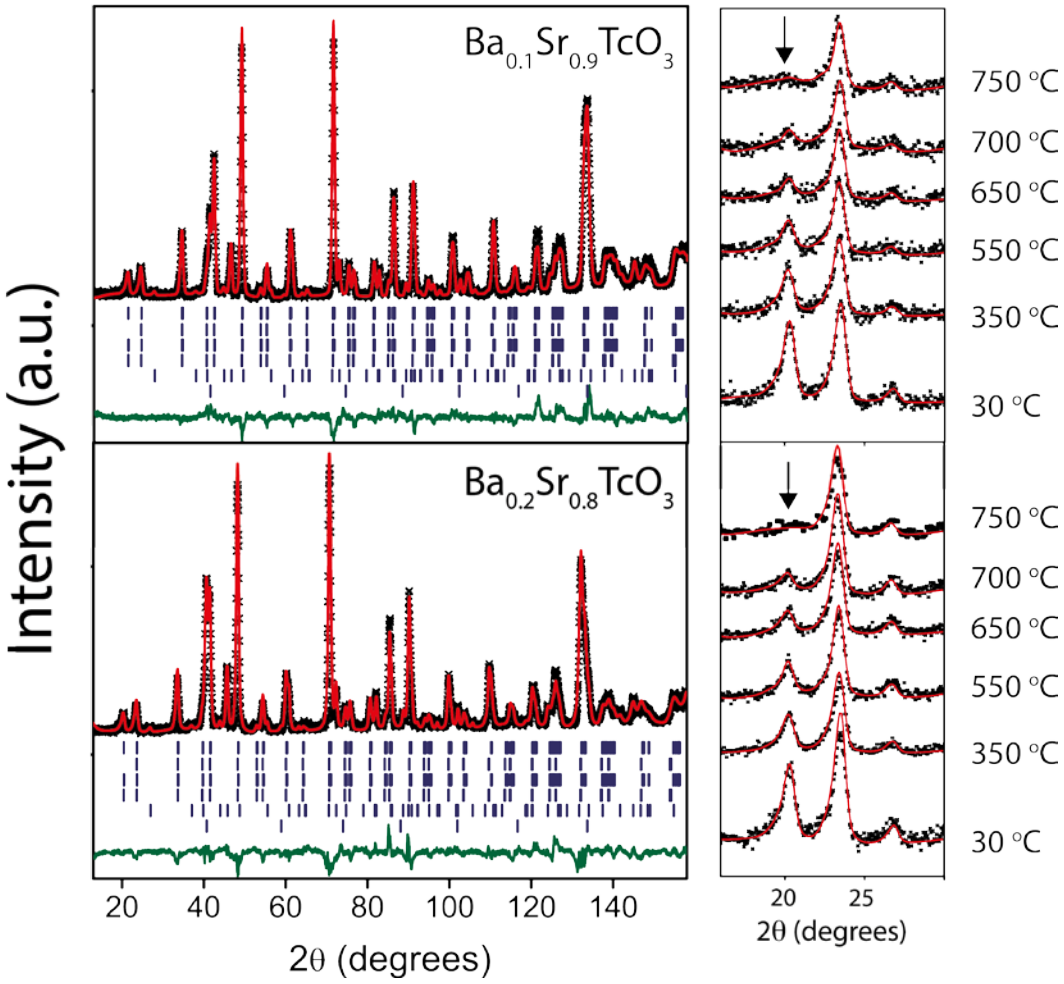

Figure 4. Left panels show room temperature NPD (λ = 1.622 Å) patterns with Rietveld refinement fits to $Ba_{0.1}Sr_{0.9}TcO_3$ and $Ba_{0.2}Sr_{0.8}TcO_3$. Right panels show the temperature dependence of the overlapping (110) and (001) magnetic peaks (indicated by the arrows).

The paucity and overlap of magnetic reflections in the NPD pattern precluded unconstrained refinement of the two magnetic structures in the Ba doped oxides. Since the magnetic moments for Tc are essentially the same in $SrTcO_3$ (1.69 μ_β) and $CaTcO_3$ (1.87 μ_β) [4, 10] and are the same in the tetragonal and orthorhombic structures of $SrTcO_3$ [6], the Tc magnetic moments in the two phases were constrained to be equal. This assumption is further supported by the observation that the incorporation of Ba in $Sr_{1-33x}Ba_xRuO_3$ did not change the magnetisation [29]. The refined Tc moments at room temperature of $Ba_{0.1}Sr_{0.9}TcO_3$ and $Ba_{0.2}Sr_{0.8}TcO_3$ are 2.32(14) μ_β and 2.11(13) μ_β, respectively. For $Ca_{0.5}Sr_{0.5}TcO_3$ the refined moment was 1.91(9) μ_β. If it was assumed that only one of the two coexisting phases was magnetic then the refined magnetic moments were unacceptably high. The temperature dependence of the intensity of the magnetic peak for the two Ba containing oxides is shown in Figure 4, whilst the thermal evolution of the refined magnetic moment is given in Figure 6.

The Nèel temperatures, estimated by fitting the temperature dependence of the magnetic moments to a function of the type $A(1-T/T_N)^{\beta}$, are 714 °C and 702 °C for $Ba_{0.1}Sr_{0.9}TcO_3$ and $Ba_{0.2}Sr_{0.8}TcO_3$, respectively. These compare to 550 and 750 °C for $Ca_{0.5}Sr_{0.5}TcO_3$ and $SrTcO_3$, respectively.

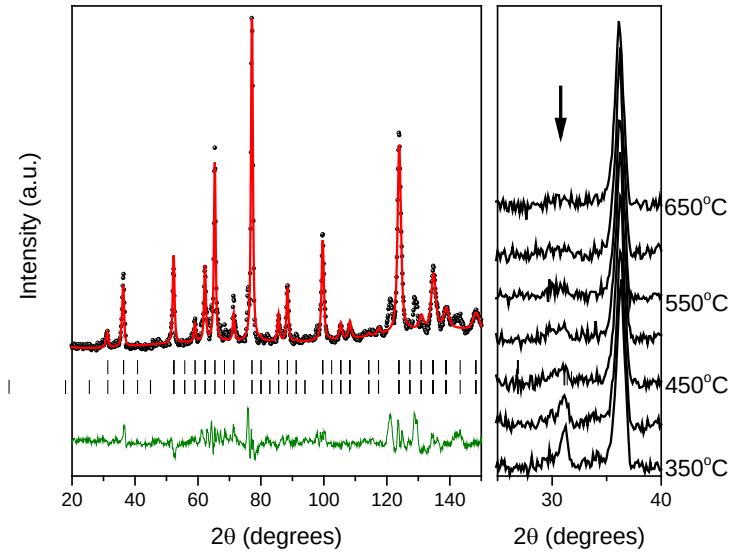

Figure 5. Left panels show room temperature NPD (λ = 2.4395 Å) patterns with Rietveld refinement fits to $Ca_{0.5}Sr_{0.5}TcO_3$. Right panels show the temperature dependence of the (110)+(001) magnetic peaks (indicated by the arrow). The unfitted peaks near 120° are from the furnace.

Discussion

In contrast to expectations, the Nèel temperature in the series $Sr_{1-x}A_xTcO_3$ (x= 0.1, 0.2) decreases with increasing Ba content. The variation of T_N on the effective ionic radius of the A-site cation (R_A) illustrated in Figure 7 is similar to that observed in the related series $ARuO_3$ [29] and $AMnO_3$ [30] and suggests the maximum magnetic ordering temperature is obtained for *A* = Sr (R_A = 1.44 Å). Furthermore, it appears for the three series that the substitution of Sr by Ca has a more dramatic impact on T_N than doping with Ba. For the Tc system, the Nèel temperatures illustrated in Figure 7 represent the compositions with lowest Ba content in each sample. In drawing this figure we have estimated R_A to corresponding to the value for the Sr-rich phase, based on the Rietveld refinements, on the assumption that T_N decreases with Ba content, as observed in the $AMnO_3$ oxides. Consequently the Sr-rich phases will have the higher T_N, and it is this that is estimated from the temperature dependence of the neutron diffraction patterns.

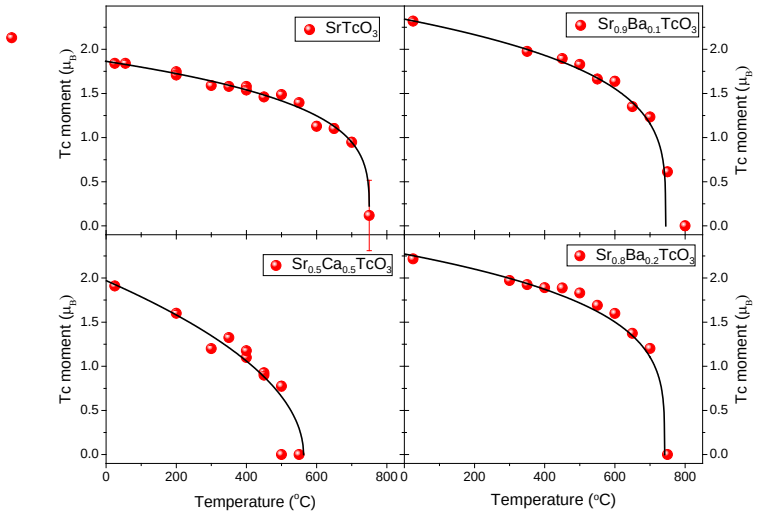

Figure 6. Temperature dependence of Tc magnetic moments for $Sr_{1-x}A_xTcO_3$ oxides as obtained from Rietveld refinements of NPD data. The solid lines serve as a guide to the eye and are calculated by the function $A(1-T/T_N)^{\beta}$ to estimate T_N.

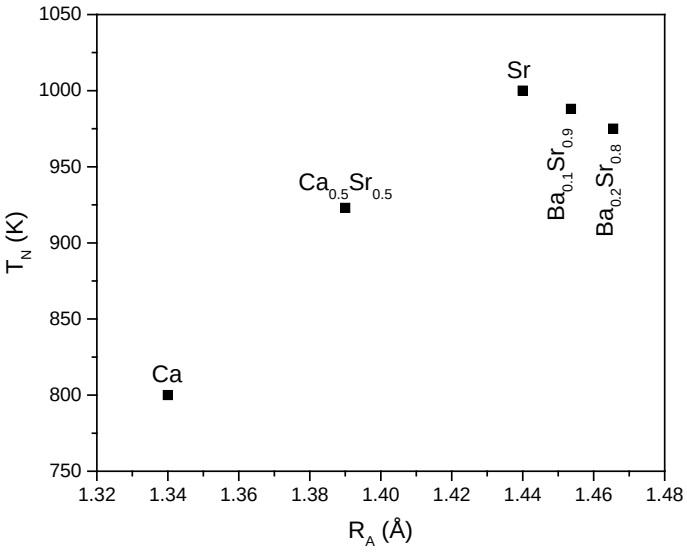

Figure 7. Variation in the Neel temperatures estimated from neutron diffraction patterns as a function of average *A*-site ionic radius for the $ATcO_3$. This figure should be compared with the published behaviour of $AMnO_3$ [30] and $ARuO_3$ [29] and illustrates that doping $SrTcO_3$ with either Ca or Ba lowers the Neel temperature.

The S-XRD patterns demonstrate that each of the $Sr_{1-x}Ba_xTcO_3$ (x = 0, 0.1, 0.2) samples transform to the ideal cubic perovskite structure well below T_N. This demonstrates that the composition dependence of the Nèel temperature is not simply a consequence of geometric changes as described by the Goodenough-Kanamori rules. To understand this it is illustrative to compare the isoelectronic Mn and Tc oxides. In the AMnO$_3$ and ATcO$_3$ series, the *B*-site cations are tetravalent and the electron configuration is $(t_{2g})^3(e_g)^0$. Both $CaTcO_3$ and $CaMnO_3$ [31] adopt an orthorhombic *Pbnm* structure and display G-type AFM ordering. It is reasonable to conclude that the difference in Nèel temperature between the two, 800 K in $CaTcO_3$ and 200K in $CaMnO_3$ [30], is a consequence of the larger extent of the 4*d* orbitals, relative to the 3*d* orbitals that enhances the Tc-O orbital overlap, which increases covalency of the Tc-O bond. In both systems, the increase in the Nèel temperature upon replacement of the Ca with Sr is ascribed to an increase in the *M*-O-*M* bond angle which strengthens the magnetic exchange interaction and results in an increase in T_N [1, 4, 6, 11, 17]. This reasoning, however, does not explain the impact of Ba doping on the behaviour of the T_N since these oxides become cubic at temperatures below T_N. Consequently the *M*-O-*M* bond angle is independent of Ba content near the Nèel temperature. To explain this we consider the related Ru ($4d^4$) perovskites. Previous studies have noted similar behaviour to that seen here for the Tc oxides in cubic members of the series $Sr_{1-x}Ba_xRuO_3$ [29], where it was suggested that Ba doping impacts the bandwidth through two opposite effects. Firstly because the *A*–O interaction competes with the Ru^{4+} ions for the O-2p(π) electrons, the stronger ionic character of the Ba^{2+}, relative to Sr^{2+}, makes it less competitive for the O-2p orbitals, which enhances the covalent admixture of O-2p(π) character into the primarily 4*d*-electron π^* bands. This broadens the bandwidth W. Alternatively, in the cubic structure Ba doping increases the unit cell parameter and hence Ru–O bond length, reducing the bandwidth. Variable pressure studies of $Sr_{1-x}Ba_xRuO_3$ demonstrate the former effect dominates with the increase in the Ru-O bond lengths only partially compensating for the broadening of the Rd 4*d* bands due to the strong ionic character of the Ba^{2+} cation [29]. It appears that the same effect is occurring in the present series, although variable pressure measurements of doped $SrTcO_3$ samples would be required to verify this. These would be extremely technically challenging, given the high Neel temperatures and radioactive nature of the samples.

In summary, polycrystalline samples of $Sr_{1-x}Ba_xTcO_3$ with ideal compositions x = 0.1, 0.2, 0.3, 0.4, together with a sample of $Sr_{0.5}Ca_{0.5}TcO_3$ were prepared for the first time. Tc K-edge XAS measurements have established that the Tc is tetravalent in all cases. S-XRD

measurements have demonstrated that the Ba doped samples are poised near a discontinuous *Imma-I*4/*mcm* transformation and that small variations in composition result in phase-separation similar to that seen in other perovskite systems including $Sr_{1-x}Pr_xMnO_3$ [25] and $BaPb_{1-x}Bi_xO_3$ [26]. Using variable temperature neutron powder diffraction it was demonstrated that, contrary to predictions, the Nèel temperature decreases with both Ba and Ca content. The behaviour of T_N in the ATcO$_3$ system mimics that observed recently in AMnO$_3$ and ARuO$_3$, but with the exception of CaTcO$_3$ the compounds are all cubic at the Neel temperature. This unequivocally demonstrates the importance of the broadening of the π^* bandwidth W by the *A*-site cation. It is hoped that these experimental sudies will inspire additional efforts to quantify the relative effects of covalency and local bond distance changes in tuning magnetic interactions in the heavier transition metal oxides.

ACKNOWLEDGMENTs. We acknowledge the assistance of Terry McLeod and Mike Jovanovic in sample preparation at ANSTO. The authors thank Mr. Trevor Low and Ms. Julie Bertoia for health physics support at UNLV. BJK acknowledges the support of the Australian Research Council. FP acknowledges the Department of Chemistry and Biochemistry at UNLV for supporting his research through a startup package. This work was, in part, performed at the powder diffraction and X-ray spectroscopy beamlines at the Australian Synchrotron.

References

1. C. L. Ma, Y. Zhu, T. C. Zang and X. D. Wang, *Physics Letters A*, 2011, **375**, 3615-3617.
2. S. Middey, A. K. Nandy, S. K. Pandey, P. Mahadevan and D. D. Sarma, *Physical Review B*, 2012, **86**, 104406.
3. J. Mravlje, M. Aichhorn and A. Georges, *Phys. Rev. Lett.*, 2012, **108**, 197202.
4. E. E. Rodriguez, F. Poineau, A. Llobet, B. J. Kennedy, M. Avdeev, G. J. Thorogood, M. L. Carter, R. Seshadri, D. J. Singh and A. K. Cheetham, *Phys. Rev. Lett.*, 2011, **106**, 067201.
5. T. Takeda and S. Ohara, *Journal of the Physical Society of Japan*, 1974, **37**, 275-275.
6. G. J. Thorogood, M. Avdeev, M. L. Carter, B. J. Kennedy, J. Ting and K. S. Wallwork, *Dalton Trans.*, 2011, **40**, 7228-7233.
7. J. M. Longo, P. M. Raccah and J. B. Goodenough, *J. Appl. Phys.*, 1968, **39**, 1327.
8. Mazin, II and D. J. Singh, *Physical Review B*, 1997, **56**, 2556-2571.
9. S. Calder, V. O. Garlea, D. F. McMorrow, M. D. Lumsden, M. B. Stone, J. C. Lang, J. W. Kim, J. A. Schlueter, Y. G. Shi, K. Yamaura, Y. S. Sun, Y. Tsujimoto and A. D. Christianson, *Phys. Rev. Lett.*, 2012, **108**, 257209.
10. M. Avdeev, G. J. Thorogood, M. L. Carter, B. J. Kennedy, J. Ting, D. J. Singh and K. S. Wallwork, *J. Am. Chem. Soc.*, 2011, **133**, 1654-1657.
11. C. Franchini, T. Archer, J. G. He, X. Q. Chen, A. Filippetti and S. Sanvito, *Physical Review B*, 2011, **83**, 220402.
12. C. M. Dai and C. L. Ma, *Modern Physics Letters B*, 2014, **28**, 1450049.
13. C. L. Ma, C. M. Dai, G. Y. Chen, D. Chen, T. C. Zang, L. J. Ge, W. Zhou and Y. Zhu, *Solid State Communications*, 2015, **219**, 25-27.
14. C. L. Ma and T. Zhou, *Physica B-Condensed Matter*, 2012, **407**, 218-221.
15. G. T. Wang, L. Li, C. Liu, M. P. Zhang and Z. X. Yang, *Physics Letters A*, 2012, **376**, 3313-3316.
16. W. Zhang and P. Q. Tong, *Journal of Physics-Condensed Matter*, 2012, **24**, 185401.
17. V. S. Borisov, I. V. Maznichenko, D. Bottcher, S. Ostanin, A. Ernst, J. Henk and I. Mertig, *Physical Review B*, 2012, **85**, 134410.
18. Y. Syono, S. I. Akimoto and K. Kohn, *Journal of the Physical Society of Japan*, 1969, **26**, 993-999.
19. O. Muller, W. B. White and R. Roy, *Journal of Inorganic & Nuclear Chemistry*, 1964, **26**, 2075-2086.
20. K. S. Wallwork, B. J. Kennedy and D. Wang, *AIP Conference Proceedings*, 2007, **879**, 879-882.
21. K. D. Liss, B. Hunter, M. Hagen, T. Noakes and S. Kennedy, *Physica B-Condensed Matter*, 2006, **385-86**, 1010-1012.
22. C. Glover, J. McKinlay, M. Clift, B. Barg, J. Boldeman, M. Ridgway, G. Foran, R. Garrett, P. Lay and A. Broadbent, *AIP Conference Proceedings*, 2007, **882**, 884-886.
23. C. J. Howard, K. S. Knight, B. J. Kennedy and E. H. Kisi, *Journal of Physics-Condensed Matter*, 2000, **12**, L677-L683.
24. B. J. Kennedy, B. A. Hunter and J. R. Hester, *Physical Review B*, 2002, **65**, 224103.
25. T. Y. Tan, N. Martin, Q. D. Zhou, B. J. Kennedy, Q. F. Gu, J. A. Kimpton, Z. M. Zhang and L. Y. Jang, *J. Solid State Chem.*, 2013, **201**, 115-127.
26. E. Climent-Pascual, N. Ni, S. Jia, Q. Huang and R. J. Cava, *Physical Review B*, 2011, **83**, 8.
27. B. J. Kennedy, M. Avdeev, H. L. Feng and K. Yamaura, *J. Solid State Chem.*, 2016, **237**, 27-31.
28. S. N. Bushmeleva, V. Y. Pomjakushin, E. V. Pomjakushina, D. V. Sheptyakov and A. M. Balagurov, *Journal of Magnetism and Magnetic Materials*, 2006, **305**, 491-496.
29. C. Q. Jin, J. S. Zhou, J. B. Goodenough, Q. Q. Liu, J. G. Zhao, L. X. Yang, Y. Yu, R. C. Yu, T. Katsura, A. Shatskiy and E. Ito, *Proceedings of the National Academy of Sciences of the United States of America*, 2008, **105**, 7115-7119.
30. O. Chmaissem, B. Dabrowski, S. Kolesnik, J. Mais, D. E. Brown, R. Kruk, P. Prior, B. Pyles and J. D. Jorgensen, *Physical Review B*, 2001, **64**, 134412.

31. Q. D. Zhou and B. J. Kennedy, *Journal of Physics and Chemistry of Solids*, 2006, **67**, 1595-1598.